Diffusion-controlled spherulite growth in obsidian inferred from H_2O concentration profiles

Jim Watkins[1], Michael Manga[1], Christian Huber[1] and Michael Martin[2]

(1) Department of Earth and Planetary Science, University of California, Berkeley, CA, USA

(2) Advanced Light Source, Lawrence Berkeley National Laboratory, Berkeley, CA, USA

Abstract Spherulites are spherical clusters of radiating crystals that occur naturally in rhyolitic obsidian. The growth of spherulites requires diffusion and uptake of crystal forming components from the host rhyolite melt or glass, and rejection of non-crystal forming components from the crystallizing region. Water concentration profiles measured by synchrotron-source Fourier transform spectroscopy reveal that water is expelled into the surrounding matrix during spherulite growth, and that it diffuses outward ahead of the advancing crystalline front. We compare these profiles to models of water diffusion in rhyolite to estimate timescales for spherulite growth. Using a diffusion-controlled growth law, we find that spherulites can grow on the order of days to months at temperatures above the glass transition. The diffusion-controlled growth law also accounts for spherulite size distribution, spherulite growth below the glass transition, and why spherulitic glasses are not completely devitrified.

Keywords Spherulites - Obsidian - FTIR - Advection–diffusion

Introduction

Spherulites are polycrystalline solids that develop under highly non-equilibrium conditions in liquids (Keith and Padden *1963*). Natural spherulites are commonly found in rhyolitic obsidian and have evoked the curiosity of petrologists for more than a century

(e.g., Judd *1888*; Cross *1891*). Over the past several decades, numerous studies on spherulite morphology (Keith and Padden *1964a*; Lofgren *1971a*), kinetics of spherulite growth (Keith and Padden *1964b*; Lofgren *1971b*), disequilibrium crystal growth rates and textures (Fenn *1977*; Swanson *1977*), and field observations (Mittwede *1988*; Swanson et al. *1989*; Manley and Fink *1987*; Manley *1992*; Davis and McPhie *1996*; MacArthur et al. *1998*, and many others) have shed light on the conditions and processes behind spherulite nucleation and growth. Despite the long-standing interest, several fundamental questions persist. For example: On what timescales do natural spherulites form? At what degree of undercooling do spherulites begin to grow? Can spherulites grow below the glass transition? Why doesn't spherulite growth lead to runaway heating? And, why are spherulites spherical? In this paper, we revisit these questions and contribute a new quantitative approach for estimating spherulite growth rates.

Qualitative description of spherulite growth

Spherulites in rhyolitic obsidian are composed primarily of alkali feldspar and SiO_2 polymorphs. Spherulites are often mm-scale, but are known to range from submicroscopic to m-scale (e.g., Smith et al. *2001*). They may be randomly distributed and completely isolated, or nucleate preferentially to form clusters or trains (e.g., Davis and McPhie *1996*). Within a deposit, spherulitic textures and relationships may vary widely owing to local differences in emplacement temperature, flow depth, cooling rate, and surface hydrology (Manley *1992*; MacArthur et al. 1998). Despite these complexities, the fact that spherulites occur almost exclusively in glasses seems to require conditions that yield slow nucleation rates yet relatively rapid crystal growth rates.

As a melt cools below the liquidus temperature (T_{eq}) for a given crystalline phase, an energy barrier must be overcome in order for the new phase to nucleate and grow. Just below T_{eq}, this energy barrier is finite and decreases with decreasing temperature. A certain amount of undercooling is always necessary to nucleate a solid phase (Carmichael et al. *1974*), where the degree of undercooling (ΔT) is the difference between the equilibrium temperature T_{eq} and the actual magmatic temperature T. In siliceous lavas,

atomic mobility is sluggish and large ΔT can be achieved prior to nucleation. Once nucleation does occur, crystal growth proceeds and crystal growth rates are dictated by the magnitude of ΔT.

Large undercoolings promote rapid crystallization, but are also associated with lower magmatic temperatures and slower elemental diffusivities. For crystals growing from a melt or glass of different composition, crystal growth rates are limited by the ability of melt components to diffuse towards or away from the crystallizing front. In the case of spherulites, it is has been shown that certain major- and trace-elements are rejected by crystallizing phases and concentrated at the spherulite–glass interface (Smith et al. *2001*).

Since the mineral phases that compose rhyolitic spherulites are nominally anhydrous, water is also rejected from the crystalline region. Among incompatible melt species, water is perhaps the most extensively studied because of its pronounced effects on magma viscosity and major-element diffusion coefficients. As a result, methods for determining water concentrations in rhyolitic glasses have been developed over the past 25 years (e.g., Stolper *1982*; Newman et al. 1986, Zhang et al. *1997*) using Fourier transform infrared spectroscopy (FTIR). The goal of our measurements is to use FTIR to resolve water concentration gradients at the spherulite–glass interface with high spatial resolution (see Castro et al. *2005*) to better understand the growth history of spherulites.

Sample descriptions

The spherulites analyzed in this study are from a hand sample of a rhyolitic vitrophyre that lies in the Quaternary Tequila volcanic field, western Mexico. Lavas that range in composition from basalt to rhyolite surround an andesite stratovolcano (Volcán Tequila) that formed about 200 kyr ago (Lewis-Kenedi et al. *2005*). The rhyolites and obsidian domes are among the earliest erupted units, ranging in age from 0.23 to 1.0 Ma (Lewis-Kenedi et al. *2005*).

Figure 1 is a photograph of the obsidian hand sample used in this study. The matrix is a dark, coherent glass that has not undergone post-magmatic hydration. It contains some visible but subtle “flow bands” reflecting shear flow of magmatic parcels containing

variable microlite content (Gonnermann and Manga *2003*). Isolated, light grey spherulites cross-cut flow bands and exhibit a range of sizes that are distributed homogeneously (Fig. 1).

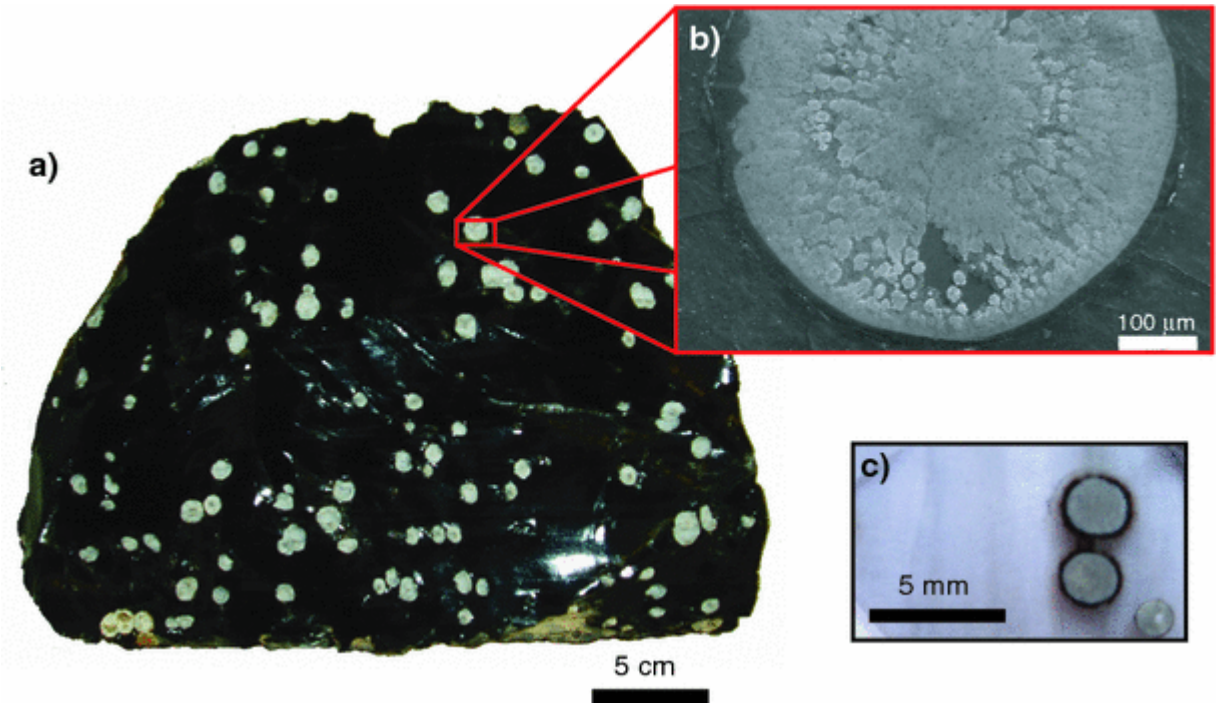

Fig. 1 **a** Photograph of a spherulitic obsidian from Tequila volcano. Spherulites ranging in size from 1.0 to 8.0 mm in diameter are distributed homogeneously throughout. **b** Cathodilluminescence image showing fibrous alkali-feldspar crystals enclosed by oblate cristobalite masses within an individual spherulite. **c** Thin section image showing spherulites cross-cutting subtle flow bands

Individual spherulites are host to three crystalline phases: 55–65% (by volume) feldspar fibers, ~30–40% oblate cristobalite masses, and <1% Fe- and Ti-oxides. The feldspar fibers are arranged in a radial habit about a central nucleus and are enclosed by the cristobalite masses. X-ray diffraction patterns indicate the feldspar is some form of alkali feldspar, but an exact determination could not be made. There is also a significant amount of void space due to the ~10% volume contraction associated with crystallization, which we neglect in our calculations.

Sample preparation and measurements

Four rectangular billets (~21 mm × 38 mm) of spherulitic obsidian were cut from a hand sample (Fig. 1) to be prepared for FTIR analysis. Each billet was ground down until at least one spherulite was sectioned through its center. The surface with the spherulite was polished to ~0.25 μm. The polished surface was mounted on a glass slide with epoxy and the billet was cut to a thickness of ~300 μm. The grinding and polishing procedure was repeated on the opposite surface to obtain a doubly polished wafer. Each of the samples was of uniform thickness (±<5% as determined by a digital micrometer with a precision of ±2 μm) so that infrared absorption data could be compared throughout the sample. Polished surfaces were necessary for minimizing infrared scattering and obtaining quality absorbance data.

Water concentration measurements were made by synchrotron-source FTIR at the Advanced Light Source at Lawrence Berkeley National Laboratory. The instrument used was a Nicolet 760 FTIR spectrometer interfaced with a Spectra-Tech Nic-Plan IR microscope capable of spot sizes of 3–10 μm (Martin and McKinney *1998*). Transects were oriented perpendicular to spherulite rims and measurements were made on the surrounding glassy matrix. Total water concentrations were determined from the intensity of the 3,570 cm^{-1} peak (Newman et al. *1986*), which reflects the abundance of hydrous species (XOH) including molecular water (HOH). Hereafter, we refer to all hydrous species collectively as "water". Analytical error is estimated to be ±0.005 wt% based on repeated measurements.

Figure 2 shows data from a transect between two adjacent spherulites. At the rim–matrix interface of each spherulite, there is a local maximum in water content that decreases with distance into the surrounding matrix to background levels (~0.115 wt% in this case). Similar profiles were measured on seven spherulites ranging in size from 1.7 to 5.2 mm in diameter.

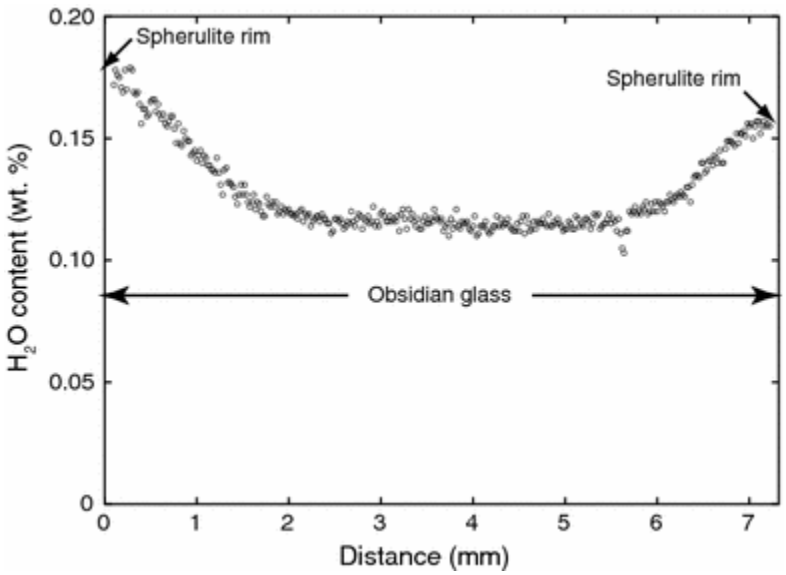

Fig. 2 FTIR transect between two spherulites of different size illustrating the expulsion of water into the surrounding melt or glass during spherulite growth

One of the samples was also analyzed using a Cameca SX-51 electron microprobe to characterize major-element variations. Due to the similarity in bulk composition between spherulites and their host, gradients in major elements could not be resolved quantitatively within detection limits. However, qualitative variations are resolved through detailed WDS X-ray mapping for three major elements taken on an individual spherulite (Fig. 3). A close look at the rim–matrix interface reveals a relative depletion in crystallizing components K and Si and concomitant enrichment in Na.

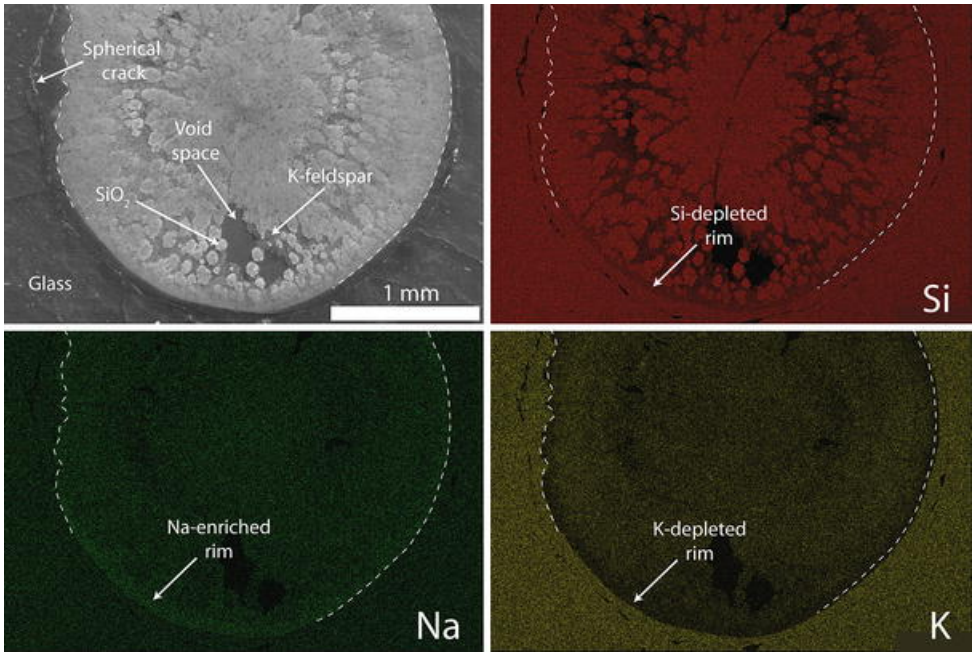

Fig. 3 Cathodilluminescence image of a spherulite (*upper left*) and electron microprobe element maps on the same spherulite. *Dark regions* correspond to relatively low concentrations. Note the relative enrichment in Na and depletion in K and Si at the spherulite boundary

Interpretation

Spherulite growth from a liquid or glass of different composition requires diffusion of crystal-forming components, which become depleted over diffusive lengthscales around the crystallizing region. Figures 2 and 3 clearly illustrate this process and confirm that impurities are not trapped within crystals or interstitial voids. The outward rejection of water induces a concentration gradient down which water diffuses into the surrounding matrix, resulting in profiles like that shown in Fig. 2.

For four of the seven spherulites analyzed, the data were clean enough to demonstrate that >95% of the water from the volume occupied by the spherulite could be accounted for in the water diffusion profile. This is noteworthy because it provides a stoichiometric relationship between the moles of water removed and moles of sanidine (or cristobalite) crystallized within the spherulite volume, thus allowing water rejection and diffusion to be used as a proxy for spherulite growth.

Model for spherulite growth

With each increment of spherulite growth, a known amount of water is expelled ahead of the advancing crystalline front. In this way, water diffusion into the matrix is in competition with the propagating spherulite boundary. Here we present a model that tracks the expulsion and diffusion of water during spherulite growth in the reference frame of the expanding spherulite rim. In this reference frame, the profiles in Fig. 3 can be modeled by solving numerically the advection–diffusion equation:

$$\frac{\partial C}{\partial t} - \mathbf{u} \cdot \nabla C = \nabla \cdot [D_{OH} \cdot \nabla C] \quad (1)$$

where C is the concentration of water, $\mathbf{u}$ is the velocity of the growing interface, and $D_{OH}(C,T,P)$ is the diffusivity of water in rhyolite melt or glass. Zhang and Behrens (*2000*) showed that $D_{OH}(C,T,P)$ varies linearly with water concentration at low total water contents (less than about 2 wt%), and we account for this effect in our model. However, we do not include variations in $D_{OH}(C,T,P)$ with temperature and pressure—a simplifying assumption discussed later. Taking advantage of the spherical symmetry of spherulites, (1) can be simplified and expressed as a function of the radial distance only:

$$\frac{\partial C}{\partial t} - u_r \frac{\partial C}{\partial r} = D_{OH}(r) \quad (2)$$

where D_{OH} is updated at the beginning of each timestep. The velocity of the interface u_r ($u_r = dR/dt$ where R is the radius of the spherulite) is given by the choice of spherulite growth law. Keith and Padden (*1963*) found experimentally that at constant temperature, spherulites in polymer liquids generally grow according to a linear growth law whereby u_r is constant and R scales with time as t:

$$u_r = n \cdot D_{OH} \quad (3)$$

where n is a free parameter that represents the competition between spherulite growth and water diffusion.

A possible alternative is a diffusion-controlled growth law (Granasy et al. *2005*), whereby the radius scales with time as $t^{1/2}$:

$$u_r = a \cdot \left(\frac{D_{OH}}{t}\right)^{1/2} \quad (4)$$

where a is a free parameter analogous to n in the linear case.

The appropriate boundary conditions for this problem are: (1) fixed concentration of water far from the growing interface and (2) time-dependent concentration of water at the rim–matrix interface that is related to the flux of water expelled during each increment of growth. The second boundary condition is implemented by ensuring mass conservation:

$$\int_{R(t)}^{R_\infty} (C(r,t) - C_\infty) r^2 dr = \frac{1}{3} C_\infty R(t)^3 \tag{5}$$

where $C(r,t)$ is the concentration of water at a distance r from the center of the spherulite, R is the spherulite radius, and C_∞ represents the background concentration of water at some distance R_∞ into the surrounding matrix. Equation (5) states that the water represented under the diffusion profile is equal to 100% of the water that once occupied the spherulite volume. Any difference between these two values is used to update $C(R,t)$ after each timestep so that the equality is true. Figure 4 is a schematic illustration of the model setup.

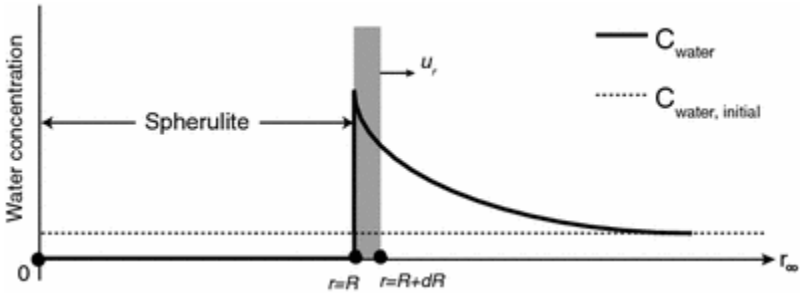

Fig. 4 Schematic diagram summarizing the 1D spherulite growth and water diffusion model. The *dark black line* represents actual (time-dependent) water concentration and *dashed line* represents the initial water concentration. The width of the *vertical gray bar* represents an increase in spherulite radius from R to $R + dR$, and the water within this region is removed and fluxed into the new boundary at $R + dR$. The model assumes perfectly efficient water expulsion

Results

The temporal evolution of model water concentration profiles depends strongly on the choice of growth law. Figure 5 compares model profiles using both the linear growth law (5a) and the diffusion-controlled growth law (5b) as a function of spherulite radius (i.e.,

time). In the linear regime, the concentration of water at the growing spherulite boundary increases progressively with time. This is a consequence of the spherical geometry, wherein the volume of water expelled increases with each (constant) growth increment d*R*. By contrast, in the diffusion-controlled regime the diffusion of water counterbalances the time-dependent growth increment d*R* such that the concentration of water at the spherulite boundary remains relatively constant with time.

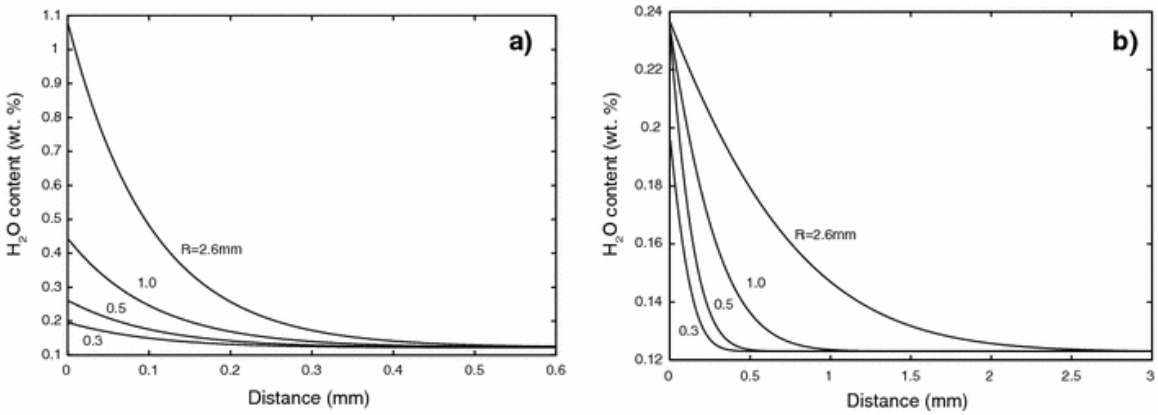

Fig. 5 Model calculations showing the evolution of water concentration away from spherulite boundaries assuming two different spherulite growth laws. Note the different scales for the *x*- and *y*-axes. The linear growth law (5a) leads to narrow profiles with a progressive build-up of water at the edge of the spherulite whereas the diffusion-controlled growth law (5b) leads to wider profiles and nearly steady values of water concentration at the spherulite edge

Figure 6 compares model results to measured profiles from two spherulites of different size. The two profiles are representative of those measured in this study and include the largest and smallest spherulites examined. Figure 6a, b corresponds to data from a spherulite of radius 0.86 mm, while Fig. 6c, d correspond to data from a spherulite of radius 2.6 mm. The figures on the left (Fig. 6a, c) assume linear growth whereas the figures on the right (Fig. 6b, d) assume diffusion-controlled growth. Although the agreement between model curves and measured profiles is not very satisfying, it is clear that an equally good (or, for that matter, equally poor) fit can be achieved using either growth law for a given spherulite. However, there is one important distinction between the two growth models. Figure 6a, c shows that a smaller coefficient *n* is required in going from the smaller to the larger spherulite. In contrast, Fig. 6b, d shows that a larger

coefficient *a* is required in going from the smaller spherulite to the larger spherulite. The significance of this is discussed in the next section.

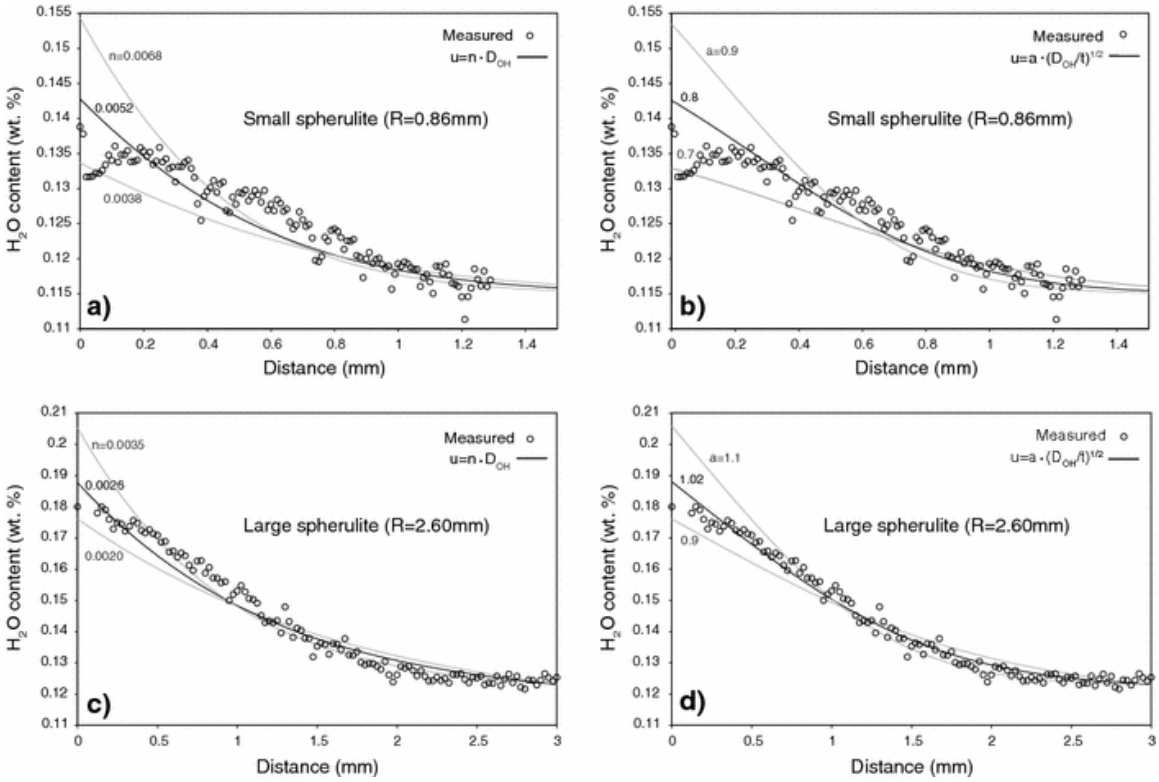

Fig. 6 Comparison between measured water concentration profiles and model calculations. **a** and **c** show results for two different spherulites using a linear growth law (i.e., $u \sim D_{OH} \cdot t$). **b** and **d** show results for two different spherulites using a diffusion-controlled growth law (i.e., $u \sim (D_{OH}/t)^{1/2}$). Clearly, indistinguishable results can be obtained using either growth law for a spherulite of given radius. *Dark curves* represent initial conditions for post-growth diffusion (see text), which leads to the profiles in Fig. 7

A striking feature of all measured water concentration profiles is the "flattening" they exhibit near the rim–matrix interface, which may be attributed to post-growth diffusion of water. In order to account for this effect, we use the bold profiles from Fig. 6 as the initial condition for the post-growth model, and, as $dR/dt = 0$, (2) reduces to the diffusion equation with no-flux boundary conditions (i.e., water is not allowed to diffuse back into the spherulite). Results are summarized in Fig. 7 for the small and large spherulite. The duration of post-growth diffusion (in years) depends on D_{OH} (i.e., temperature), and the values quoted in Fig. 7 arbitrarily assume $T = 400°C$. A lower temperature would simply require more prolonged post-growth diffusion in order to achieve an identical fit. The two most important points that arise from Fig. 7 are: (1) the agreement between measured and

model profiles is markedly improved with inclusion of post-growth diffusion, and (2) the same duration of post-growth diffusion is required to fit profiles for both large and small spherulites.

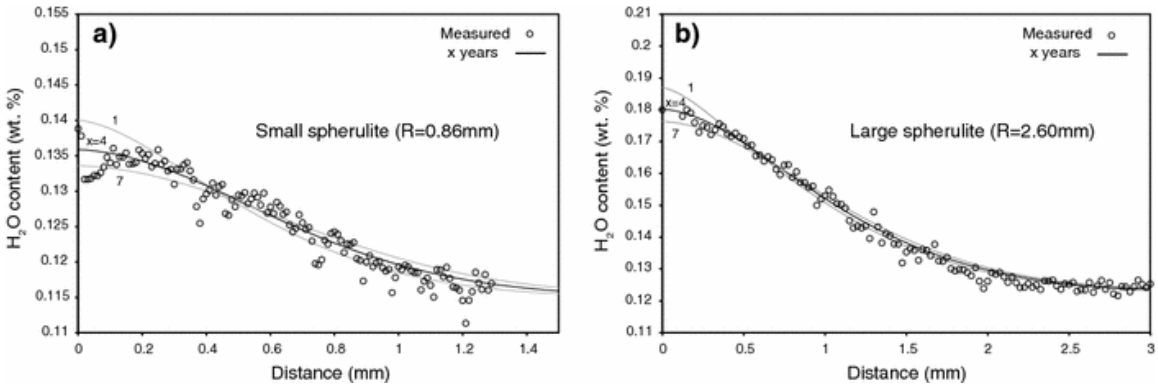

Fig. 7 Data versus model profiles after post-growth diffusion of water is included. Initial conditions are bold profiles in Fig. 6. The timescales correspond to the lower bound of the experimentally determined D_{OH} (i.e., T = 400°C; Zhang and Behrens *2000*). The same duration of post-growth diffusion is required to fit profiles for both large and small spherulites, which is expected assuming a common closure temperature for spherulites from a given locality

Discussion

The distinction between linear and diffusion-controlled growth laws is important as it pertains to several questions presented earlier about natural spherulites. Keith and Padden (*1964b*) studied spherulite growth kinetics under isothermal conditions in a range of polymer liquids and found that impurities often become trapped in the interstices of the crystalline region. Under these circumstances, impurities do not influence subsequent crystal growth and spherulite growth rates are linear in time (Keith and Padden *1964b*). However, the linear growth law breaks down when rejected species are sufficiently mobile. That is, when diffusion of impurities occurs on the same timescale as crystal growth rates, the concentration of impurities at the crystalline interface increases progressively. As a consequence, spherulite growth rates decrease with spherulite size owing to the reduction in local concentrations of crystallizing components. Hence, we interpret the observation of rejected impurities outside the crystalline volume as evidence

in itself for nonlinear growth kinetics. As discussed by Keith and Padden (*1964b*), the onset of nonlinear growth is favored by reducing the molecular weight of the impurity or by increasing the crystallization temperature to reduce the driving force for crystallization and to enhance impurity diffusivities. Water, the impurity of interest for natural spherulites, satisfies these conditions: it is relatively mobile, depresses the rhyolite liquidus, and enhances the diffusivity of other melt components.

An additional argument can be made for diffusion-controlled growth from the results presented in Figs. 6 and 7. The model curves in Fig. 7 indicate that both spherulites experienced the same duration of post-growth diffusion of water, and hence, stopped growing at the same time or temperature. Intuitively, one would expect that the larger spherulite began growing earlier at higher temperatures—a possibility that is not explicitly accounted for in our model. Note, however, that we assume constant a, n, and D_{OH} (constant with respect to temperature). Of these parameters, D_{OH} is the only one that is likely to change with temperature during spherulite growth. The observed differences in a and n between spherulites may thus represent changes in D_{OH} with temperature. In the diffusion-controlled growth model, a larger a translates into a higher average D_{OH} (i.e., temperature) for the larger spherulite ($a = 1.02$) versus the smaller spherulite ($a = 0.8$), consistent with the expectation stated above. In contrast, if we assume a linear growth law, comparable fits between the larger spherulite ($n = 0.0026$) and smaller spherulite ($n = 0.0052$) correspond to lower temperatures (i.e., slower average growth rate) for the larger spherulite, which is difficult to reconcile with the assumption that both spherulites stopped growing at the same temperature. Indeed, using a slightly different modeling approach, Castro et al. (*2008*) found that larger spherulites experienced higher average growth rates than smaller spherulites. In their paper, however, this result was attributed to size-dependent growth rates versus our suggestion here that this reflects different temperature histories (i.e., temperature-dependent growth rates).

Diffusion-controlled growth also has implications for the size distribution of spherulites. For instance, we should expect a greater abundance of larger spherulites because rapid initial growth allows smaller spherulites to catch up in size to those earlier-forming,

larger spherulites. Qualitatively, this seems to be the case for our samples. However, no attempt was made to statistically analyze spherulite sizes because of the limited size of our hand sample and the challenge of sectioning spherulites through their center.

On what timescales do natural spherulites form?

Using water rejection as a proxy for crystallization rates, it is possible to calculate timescales for spherulite growth. This requires knowledge of the diffusivity of water (D_{OH}) during spherulite formation, and one obvious shortcoming of the model is the assumption that D_{OH} is fixed in a rhyolite undergoing cooling. Nevertheless, we calculate isothermal spherulite growth rates to bracket the true timescales for spherulite formation. Using D_{OH} in rhyolite at conditions relevant to our samples (~0.1 wt% water and 0.1 MPa; Zhang and Behrens *2000*), the time required to grow a spherulite of given radius comes from the scaling relationship

$$t \sim \frac{R^2}{D_{OH}} \tag{6}$$

where R is the final radius of the spherulite. Results are summarized in Fig. 8, which shows the time required for a spherulite to reach a given radius at various fixed temperatures. For simplicity, these calculations assume that D_{OH} is not dependent on water concentration. We justify this by noting that these values are within a factor of 2 to the values we calculate from our full advection–diffusion model for radii greater than about 1 mm.

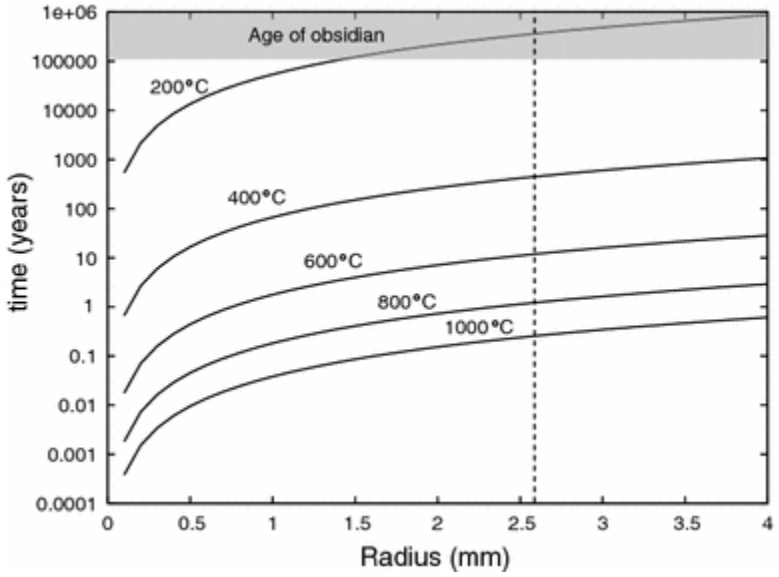

Fig. 8 Time required to grow a spherulite of given radius at various fixed temperatures assuming a diffusion-controlled growth law (6) and using a proportionality constant of $a = 1.0$. The *shaded region* at the *top* of the graph encompasses the range of possible ages for the host obsidian (Lewis-Kenedi et al. 2005) and the *dashed line* indicates the size of the largest spherulite analyzed in this study. For spherulites to grow appreciably on cooling timescales, they must form at temperatures above about 400°C

According to the diffusion-controlled growth model, a spherulite of 2.6 mm requires ~300 days at 800°C, ~10 years at 600°C, or ~300 years at 400°C. These timescales are consistent with spherulites forming at temperatures above 600°C in parts of lava flows that cool on the order of years to decades in heat flow models that assume instantaneous emplacement of lava followed by static cooling (Manley *1992*; Manley and Fink *1987*). At temperatures below about 400°C, diffusion-controlled growth is extremely sluggish and we consider $T = 400$°C an approximate lower bound for spherulite growth during cooling. This can explain the absence of macroscopic spherulites along quench margins where rapid cooling has minimized the duration of high temperature growth rates. Of course, better estimates for timescales of spherulite growth require additional constraints on the temperature of spherulite formation and the cooling history of their host.

At what degree of undercooling do spherulites begin to grow?

Emplacement temperatures for rhyolite vary considerably (790–925°C; Carmichael et al. *1974*). At the time of emplacement, an anhydrous rhyolite lava may be significantly undercooled, as the liquidus in this system is ~1,000°C (Ghiorso and Sack *1995*). Owing to nucleation lag times, which may be on the order of tens of years (Manley *1992*), the degree of undercooling at which nucleation actually occurs is difficult to constrain. Nevertheless, textural relationships can provide a first-order estimate. For example, crystal morphologies have been shown to correlate with the degree of undercooling in the $NaAlSi_3O_8$–$KAlSi_3O_8{\cdot}H_2O$ system (Fenn *1977*). Feldspars grown in this system formed as (1) isolated tabular crystals at low undercoolings ($\Delta T < 40$°C), (2) coarse, open spherulites at moderate undercoolings ($\Delta T \sim 75$–145°C), and (3) fine, closed spherulites at higher undercoolings ($\Delta T \sim 245$–395°C) (Fenn *1977*). This latter group of textures corresponds to the spherulites pictured in Fig. 1. From this information, a minimum ΔT on the order of 150°C (corresponding to a maximum $T = 850$°C) seems reasonable for the onset of spherulite growth, providing a minimum growth time of ~100 days. Larger ΔT associated with longer nucleation lag times are certainly possible and are probably common given that spherulites are generally smaller than the cooling timescales of decades would otherwise allow.

Do spherulites grow below the glass transition?

The glass transition signals an abrupt change in the physical properties of a melt, namely a change from liquid-like to solid-like behavior. The temperature at which this takes place depends on composition and cooling rate. For anhydrous rhyolite, the glass transition temperature (T_g) lies somewhere between 620 and 750°C (based on values in Swanson et al. *1989*; Manley *1992*; Westrich et al. *1988*), and it has been suggested that T_g may provide a minimum temperature for spherulite growth (Ryan and Sammis *1981*; Manley *1992*; Davis and McPhie *1996*). Indeed, certain field observations such as deformation of spherulites (Mittwede *1988*), boudinage of flow bands by spherulites (Manley *1992*; Stevenson et al. *1994*), and inflation of lithophysal cavities (Swanson et al. *1989*) suggest that spherulite growth takes place in melts above T_g. However, these features are not always observed. The spherulites used in this study, for instance, are

underformed and cross cut flow bands, raising the possibility that they grew, at least in part, below the glass transition.

Since we assume that spherulite growth is governed by diffusion of components across spherulite boundaries, the question of whether spherulites grow below T_g is really a question of how elemental diffusivities are affected by the glass transition. Based on the study by Zhang and Behrens (*2000*), the diffusivity of water appears to vary smoothly across the glass transition. Figure 9 shows diffusivities for other various chemical species in rhyolitic obsidian as a function of temperature. Across the range of possible glass transition temperatures, there is no evidence for significant changes in the diffusivity mechanisms for any of the components shown. This is consistent with the notion that rhyolite liquids are structurally similar to rhyolite glasses, as evidenced by only minor changes (~5%) in heat capacity across the glass transition (Neuville et al. *1993*). Hence, there is no reason to believe that the glass transition represents an abrupt barrier to spherulite growth. However, it is apparent from the diffusion-controlled growth model that growth rates become prohibitively slow below about 400°C.

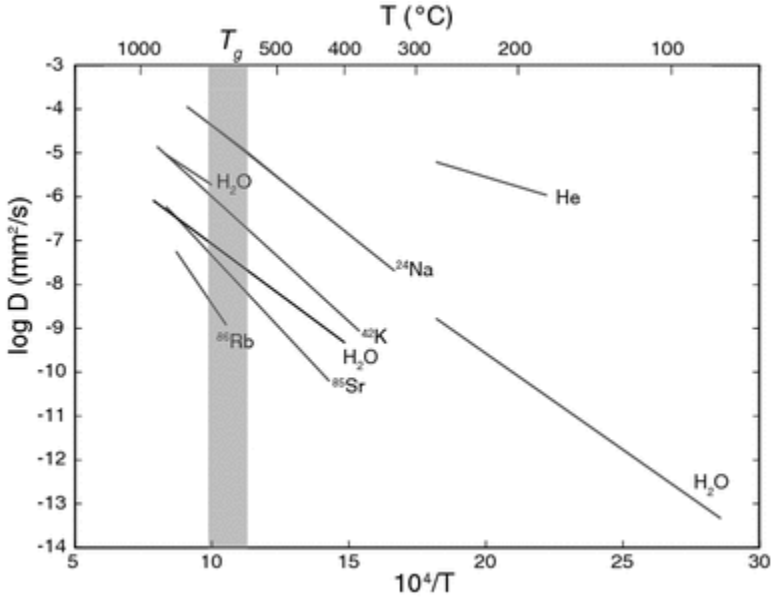

Fig 9 Temperature-dependence of diffusivities for various chemical species in obsidian. *Dark line* for H_2O is from Eq. (12) in Zhang and Behrens (*2000*) and *grey lines* for H_2O are from obsidian hydration experiments (see Freer *1981*). All other lines are from the compilation by Freer (*1981*). The main point is that major- and trace-element diffusivities appear to be insensitive to the glass transition in melts of rhyolitic composition (region shown in *grey*)

Why doesn't spherulite growth lead to runaway heating?

An issue we have not yet addressed is the release and transport of latent heat as spherulitic crystallization progresses (cf. Lofgren *1971a*). Diffusion of latent heat into the surrounding matrix could insulate growing spherulites, prolonging their exposure to elevated temperatures. Latent heat could also, in principle, lead to increased growth rates and the release of more latent heat in a positive feedback loop (Carmichael, personal communication). Obviously, this runaway heating does not take place since almost all spherulite-bearing rocks are vitrophyric. In order to explain this, we again turn to diffusion-controlled growth. We have already shown that spherulite growth is limited by the mobility of chemical species, and that spherulite growth rates proceed on the same timescale as water diffusion rates. A maximum D_{OH} of about 10^{-6} mm^2/s in rhyolite corresponds to T = 850°C. This is seven orders of magnitude lower than thermal diffusivity in obsidian, which is on the order of 10^{-1} mm^2/s over the temperature range 0–800°C (Riehle et al. *1995*). Hence, latent heat is carried away long before it can influence spherulite growth rates.

Why are spherulites spherical?

Natural spherulites are host to multiple crystalline phases with very different individual morphologies (Fig. 1). On the whole, however, spherulites are almost perfectly spherical. The simplest explanation is that their host glass or melt is homogeneous, thus offering no preferred direction in which to grow. As we noted earlier, however, some spherulites cross cut bands of textural and compositional heterogeneities (Gonnermann and Manga *2003*). An alternative explanation can be found by invoking sufficiently rapid diffusion of water.

As spherulites grow outwards and water is rejected into the surrounding matrix, there is a local reduction in the relative abundance of crystal-forming components. Since water content decreases with distance (over diffusion lengthscales) from the spherulite rim, any crystalline protrusion will grow into a melt at a higher supersaturation (i.e., higher undercooling) and respond by growing faster. This runaway effect can lead to dendritic

crystals or “cellular” morphologies (Kirkpatrick *1975*). However, there is an increase in surface energy associated with breaking the spherical symmetry of a growing spherulite. The stability of a spherical interface with finite surface tension is determined by a competition between growth rate and diffusion rate. At low growth rates, surface tension and diffusion act to maintain a minimum surface energy configuration (i.e., spherical). With increasing growth rate, however, there comes a critical point described by the Mullins–Sekerka instability at which diffusion and surface tension can no longer prohibit dendritic growth (Mullins and Sekerka *1963*; Langer *1980*). As one might expect, the transition from spherical to dendritic morphology depends on the diffusion length over which the crystallizing components are depleted. Qualitatively, for large diffusion lengths the increase in supersaturation surrounding a protrusion is minor compared to the rest of the spherulite. In this regard, we attribute the sphericity of spherulites in our samples to the high mobility of water (in relation to reaction kinetics) throughout their growth history.

Conclusions

Water concentration profiles adjacent to spherulite rims provide information about the growth history of spherulites in rhyolitic vitrophyres. We have shown that these profiles can be modeled assuming a combination of diffusion-controlled spherulite growth kinetics and post-growth diffusion of water. Qualitatively, this model can resolve temperature differences at which different spherulites grew and it accounts for why spherulites are spherical. We find that the glass transition is not a barrier to spherulite growth because chemical diffusivities are not sensitive to this transition. Furthermore, because thermal diffusivities are much faster than chemical diffusivities, spherulite crystallization does not lead to runaway heating and complete crystallization or devitrification of rhyolitic vitrophyres.

Our model also provides timescales for spherulite growth. Swanson (*1977*) was the first to show that crystals can grow to large sizes (mm-scale) on surprisingly short timescales (on the order of days) in systems with more than one phase. We have inferred that this holds true in the natural setting where spherulites can grow to large sizes on the order of

days at eruptive temperatures. However, spherulite growth rates decrease exponentially with temperature and become prohibitively slow at temperatures below about 400°C.

Lastly, we emphasize that the results presented here are based on spherulites from a single locality. A similar approach applied to spherulites from elsewhere will be useful in the future. In particular, we would like to compare timescales of during- and post-growth diffusion of water between spherulites that experienced different cooling histories. Information such as this may lead to an explanation for how and when spherulite growth and water diffusion become decoupled.

Acknowledgments We would like to thank Ian Carmichael for providing samples and suggesting that spherulites were interesting and important. We also thank the Advanced Light Source and Kent Ross for providing outstanding technical support for FTIR and microprobe measurements, respectively. This work was supported by NSF grant EAR-0608885.

References

Carmichael I, Turner F, Verhoogen J (1974) Igneous petrology. McGraw-Hill, New York, p 739

Castro J, Manga M, Martin M, (2005) Vesiculation rates of obsidian domes inferred from H_2O concentration profiles. Geophys Res Lett 32:L21307

Castro J, Beck P, Tuffen H, Nichols A, Dingwell D, Martin M (2008) Timescales of spherulite crystallization in obsidian inferred from water concentration profiles. Am Mineral (submitted)

Cross W (1891) Constitution and origin of spherulites in acid eruptive rocks. Philos Soc Wash Bull 11:411–449

Davis B, McPhie J (1996) Spherulites, quench fractures and relict perlite in a Late Devonian rhyolite dyke, Queensland, Australia. J Volcanol Geotherm Res 71:1–11

Fenn P (1977) The nucleation and growth of alkali feldspars from hydrous melts. Can Mineral 15:135–161

Freer R (1981) Diffusion in silicate minerals and glasses: a data digest and guide to the literature. Contrib Mineral Petrol 76:440–454

Ghiorso M, Sack R (1995) Chemical mass transfer in magmatic processes. IV. A revised and internally consistent thermodynamic model for the interpolation and extrapolation of liquid–solid equilibria in magmatic systems at elevated temperatures and pressures. Contrib Mineral Petrol 119:197–212

Gonnermann H, Manga M (2003) Explosive volcanism may not be an inevitable consequence of magma fragmentation. Nature 426:432–435

Granasy L, Pusztai T, Gyorgy T, Warren J, Douglas J (2005) Growth and form of spherulites. Phys Rev 72:011605

Judd J (1888) On the volcanic phenomena of the eruption, and on the nature and distribution of the ejected materials, Part I. In: Symons GJ (ed) The eruption of Krakatoa committee of the royal society. Harrison & Son, London, pp 1–46

Keith H, Jr Padden F (1963) A phenomenological theory of spherulitic crystallization. J Appl Phys 34(8):2409–2421

Keith H, Jr Padden F (1964a) Spherulitic crystallization from the melt. I. Fractionation and impurity segregation and their influence on crystalline morphology. J Appl Phys 35(4):1270–1285

Keith H, Jr Padden F (1964b) Spherulitic crystallization from the melt. II. Influence of fractionation and impurity segregation on the kinetics of crystallization. J Appl Phys 35(4):1286–1296

Kirkpatrick R (1975) Crystal growth from the melt: a review. Am Mineral 60(9–10):798–814

Langer J (1980) Instabilities and pattern formation in crystal growth. Rev Mod Phys 52:1–27

Lewis-Kenedi C, Lange R, Hall C, Delgado-Grenados H (2005) The eruptive history of the Tequila volcanic field, western Mexico: ages, volumes, and relative proportions of lava types. Bull Volcanol 67:391–414

Lofgren G (1971a) Spherulitic textures in glassy and crystalline rocks. J Geophys Res 76:5635–5648

Lofgren G (1971b) Experimentally produced devitrification textures in natural rhyolite glass. Geol Soc Am Bull 82:553–560

MacArthur A, Cas R, Orton G (1998) Distribution and significance of crystalline, perlitic and vesicular textures in the Ordovician Garth Tuff (Wales). Bull Volcanol 60:260–285

Manley C (1992) Extended cooling and viscous flow of large, hot rhyolite lavas:

implications of numerical modeling results. J Volcanolgy and Geotherm Res 53:27–46

Manley C, Fink J (1987) Internal textures of rhyolite flows as revealed by research drilling. Geology 15:549–552

Martin M, McKinney W (1998) The first synchrotron infrared beamlines at the advanced light source: microspectroscopy and fast timing. Proc Mater Res Soc 524:11

Mittwede S (1988) Spherulites in the Spring Branch Rhyolite, Western Saluda County, South Carolina. South Carolina Geol 32:21–25

Mullins W, Sekerka R (1963) Morphological stability of a particle growing by diffusion or heat flow. J Appl Phys 34:323–329

Neuville D, Courtial P, Dingwell D, Richet P (1993) Thermodynamic and rheological properties of rhyolite and andesite melts. Contrib Mineral Petrol 113:572–581

Newman S, Stolper E, Epstein S (1986) Measurement of water in rhyolitic glasses: calibration of an infrared spectroscopic technique. Am Min 71:1527–1541

Riehle J, Miller T, Bailey R (1995) Cooling, degassing and compaction of rhyolitic ash flow tuffs: a computational model. Bull Volcanol 57:319–336

Ryan M, Sammis C (1981) The glass transition in basalt. J Geophys Res 86:9515–9535

Smith R, Tremallo R, Lofgren G (2001) Growth of megaspherulites in a rhyolitic vitrophyre. Am Mineral 86:589–600

Stevenson R, Briggs R, Hodder A (1994) Physical volcanology and emplacement history of the Ben Lomond rhyolite lava flow, Taupo Volcanic Centre, New Zealand. N Z J Geol Geophys 37:345–358

Stolper E (1982) Water in silicate glasses: an infrared spectroscopic study. Contrib Mineral Petrol 81:1–17

Swanson S (1977) Relation of nucleation and crystal-growth rate to the development of granitic textures. Am Mineral 62:966–978

Swanson S, Naney M, Westrich H, Eichelberger J (1989) Crystallization history of Obsidian Dome, Inyo Domes, California. Bull Volcanol 51:161–176

Westrich H, Stockman H, Eichelberger J (1988) Degassing of rhyolitic magma during ascent and emplacement. J Geophy Res 93:6503−6511

Zhang Y, Behrens H (2000) H_2O diffusion in rhyolitic melts and glasses. Chem Geol 169:243–262

Zhang Y, Belcher R, Ihinger P, Wang L, Xu Z, Newman S (1997) New calibration of infrared measurement of dissolved water in rhyolitic glasses. Geochim Cosmochim Acta 63(15):3089–3100